# Cascaded Generalized Super-Twisting Observer Design for Sensorless PMSM Drives

Jiajia Huang, Jianliang Mao, Xin Dong, Keqi Mei, Rafal Madonski, Chuanlin Zhang, *Senior Member, IEEE*

***Abstract*—This brief investigates the use of a new cascaded generalized super-twisting observer (GSTO) for sensorless permanent magnet synchronous motor (PMSM) drives. Specifically, the developed first-stage observer extracts information about internal back-EMF, and then, ensures that the estimation error converges to an arbitrarily small region within a finite time. Meanwhile, the second-stage observer reconstructs the position and speed information synchronously, which can improve the transient performance to a certain extent compared with the arctangent function calculation-based technique. The benefits of the proposed strategy lie in that the cascaded configuration of the two observers minimizes the high-frequency noise of the back-EMF reconstruction system and provides accurate estimations of rotor position and speed. Furthermore, the chattering problem commonly seen in the conventional sliding mode observer (SMO) can be avoided in the presented scheme. Experimental results validate the effectiveness of the proposed methodology.**

***Index Terms*—generalized super-twisting observer, cascaded observer, sensorless control, PMSM, chattering reduction.**

## I. Introduction

PERMANENT magnet synchronous motors (PMSMs) are widely used in industrial applications owing to their ability to operate at wide-range speeds with high power density [1]–[3]. However, the popular field-oriented control (FOC) of PMSM relies on precise rotor position information, which generally can be obtained by a position sensor such as an encoder or a resolver. However, these sensors can lead to certain issues, including decreased reliability and increased costs. Consequently, numerous researchers have shown significant interest in position-sensorless control as a superior alternative over the past few decades [4].

With the rapid development of observer design technology, a class of model-based methods is considered as an effective sensorless control scheme for PMSM drives, especially for speed regulation in medium- and high-speed regions. For these methods, the significant and challenging task is to estimate the internal back-EMF or flux accurately. Several different approaches are put forward for the back-EMF or flux associated with the fundamental excitation, including flux observers [5], model reference adaptive systems [6], sliding mode observer (SMO) [7], [8], etc. Among these promising methods, the SMO approach is widely favored for its robustness, simple structure, and fast convergence properties [9]. However, the conventional first-order SMO generally suffers from severe chattering problems due to the utilization of discontinuous control action. To tackle this issue, a low-pass filter (LPF) is typically employed to filter out the high-frequency noise in back-EMF reconstruction. Nevertheless, the introduction of LPF inevitably brings in error in position estimation, such that the additional phase compensation is definitely required in practical applications [10]. An alternative solution is to improve the structure of the traditional sliding mode algorithm, such as applying the adaptive algorithm to optimize the control gain selection [11], [12], designing a continuous control action [13], [14], etc. For continuous sliding mode control, a constructive design strategy, called generalized super-twisting algorithm, was proposed in [15].

Another challenge is to rebuild the rotor position information from the back-EMF or flux estimation. Several practical solutions include the calculation method based on the arctangent function and the design technique of Q-type phase-locked loop (Q-PLL) [16]. However, such methods are susceptible to noises and harmonics, which may highly impact the accuracy of position estimation even if the pre-designed back-EMF observations are effective. In order to improve the estimation performance, some researchers have proposed various solutions, including a Luenberger-type observer integrated with a nonlinear second-order disturbance observer [17], and a nonlinear extended state observer (ESO) to enhance robustness and dynamics in Q-PLL [18]. However, these methods can only achieve asymptotic convergence of the observation error. It has been revealed in [19], [20] that the observation performance can be further improved by employing the finite-time observer design technique.

Through the above analysis and preliminary research, to improve the accuracy of the internal back-EMF reconstruction and the capacity of rotor position-speed estimation performance, a cascaded generalized super-twisting observer (GSTO) based two-stage observer is proposed in this brief. Specifically, the first-stage observer is built for the accurate estimation of the internal back-EMF, and the second-stage observer utilizes the estimated back-EMF information to enhance the transient performance for both position and speed estimation. The main contributions can be summarized by the following two aspects:

1) A cascaded GSTO is constructed based on the generalized super-twisting algorithm for sensorless PMSM drives,

This work was supported in part by the National Natural Science Foundation of China under Grant 62173221 and Grant 62203292. (*Corresponding author: Jianliang Mao.*)

Jiajia Huang, Jianliang Mao, Xin Dong and Chuanlin Zhang are with the College of Automation Engineering, Shanghai University of Electric Power, Shanghai 200090, China (e-mail: hjjshiep@163.com; jl_mao@shiep.edu.cn; xxddong@shiep.edu.cn; clzhang@shiep.edu.cn)

Keqi Mei is with the School of Electrical and Information Engineering, Jiangsu University, Zhenjiang 212013, China (e-mail:mkq@ujs.edu.cn)

Rafal Madonski is with the Faculty of Automatic Control, Electronics and Computer Science, Silesian University of Technology, Gliwice, 44-100, Poland (e-mail:rafal.madonski@gmail.com)

which not only relieves the high-frequency noise of the internal back-EMF estimation process but also enhances the position and speed estimation accuracy.

2) The position estimation error can converge to an arbitrarily small region within a finite time by tuning the designed parameters appropriately, thus effectively ensuring robustness.

## II. PMSM Model Description

In this section, the essential dynamic model of PMSM is presented, which will serve in the construction of the proposed cascaded GSTO in the subsequent section.

### A. Stator Voltage Equations

Assuming that the eddy currents, iron saturation, and hysteresis losses are neglected in the PMSM system, then the stator voltage equations in the stationary $\alpha$-$\beta$ axes can be expressed as follows [16]:

$$\frac{d}{dt}\begin{bmatrix} i_\alpha \\ i_\beta \end{bmatrix} = -\frac{R}{L}\begin{bmatrix} i_\alpha \\ i_\beta \end{bmatrix} - \frac{1}{L}\begin{bmatrix} E_\alpha \\ E_\beta \end{bmatrix} + \frac{1}{L}\begin{bmatrix} u_\alpha \\ u_\beta \end{bmatrix} \tag{1}$$

where $u_\alpha$, $u_\beta$ and $i_\alpha$, $i_\beta$ represent the stator voltage and current in the $\alpha$-$\beta$ axes, respectively; $R$ and $L$ are the resistance and inductance of the stator winding; $E_\alpha$ and $E_\beta$ are the back-EMFs that can be depicted detailedly by

$$E_\alpha = -\omega_e \phi_f \sin\theta_e,\ \ E_\beta = \omega_e \phi_f \cos\theta_e \tag{2}$$

where $\theta_e$ is the rotor electric angle, $\omega_e$ is the rotor electric angular velocity, and $\phi_f$ is the permanent magnet flux linkage.

### B. Motion Equations

To achieve the position and speed estimations, the dynamic model of the PMSM motion control system is studied, which can be described as

$$\dot{\theta}_e = \omega_e,\ \ \dot{\omega}_e = \frac{k_t}{J} i_q^* + d \tag{3}$$

where $i_q^*$ is the $q$-axis reference current, $d$ denotes the lumped uncertainties, $J$ is the moment of inertia, and $k_t = 1.5 p_n \phi_f$ is the torque constant in which $p_n$ is the number of pole pairs.

## III. Cascaded GSTO Design

The main result of this brief, i.e., a cascaded GSTO-based two-stage observation design framework for sensorless PMSM drives is introduced in this section.

### A. Back-EMF Estimation

In the context of sensorless PMSM drives, since the precise measurement of back-EMF is usually not directly accessible, the high-performance observer is preferred to estimate the back-EMF with sinusoidal form. To this aim, according to system (1), the GSTO-based back-EMF reconstruction dynamics system can be designed as

$$\frac{d}{dt}\begin{bmatrix} \hat{i}_\alpha \\ \hat{i}_\beta \end{bmatrix} = -\frac{R}{L}\begin{bmatrix} i_\alpha \\ i_\beta \end{bmatrix} + \frac{1}{L}\begin{bmatrix} u_\alpha - \hat{E}_\alpha - u_1 \\ u_\beta - \hat{E}_\beta - u_2 \end{bmatrix}, \tag{4}$$

$$\begin{cases} u_1 = \lambda_1 \lfloor \hat{i}_\alpha - i_\alpha \rceil^a, \hat{E}_\alpha = \lambda_2 \int \lfloor \hat{i}_\alpha - i_\alpha \rceil^b dt \\ u_2 = \lambda_1 \lfloor \hat{i}_\beta - i_\beta \rceil^a, \hat{E}_\beta = \lambda_2 \int \lfloor \hat{i}_\beta - i_\beta \rceil^b dt \end{cases} \tag{5}$$

where $\lfloor s \rceil^c \triangleq |s|^c \mathrm{sign}(s),\ c \in \mathbb{R}_+$; $\hat{E}_\alpha$, $\hat{E}_\beta$, $\hat{i}_\alpha$ and $\hat{i}_\beta$ are the estimations of $E_\alpha$, $E_\beta$, $i_\alpha$ and $i_\beta$, respectively; $\lambda_1, \lambda_2 > 0$ are the design parameters, and $a \in (1/2, 1),\ b = 2a - 1$.

For enhancing the readability of the design procedure of the first-stage observer, the block diagram is depicted in Fig. 1.

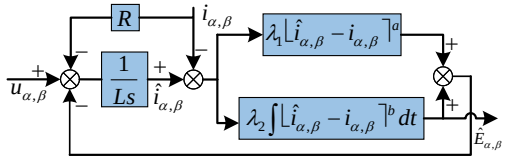


Fig. 1. Structure of back-EMF estimation using proposed GSTO.

**Remark 3.1:** Notably, the conventional SMO-based back-EMF estimation system is usually built as

$$\frac{d}{dt}\begin{bmatrix} \hat{i}_\alpha \\ \hat{i}_\beta \end{bmatrix} = -\frac{R}{L}\begin{bmatrix} i_\alpha \\ i_\beta \end{bmatrix} + \frac{1}{L}\begin{bmatrix} u_\alpha - \lambda \mathrm{sign}(\hat{i}_\alpha - i_\alpha) \\ u_\beta - \lambda \mathrm{sign}(\hat{i}_\beta - i_\beta) \end{bmatrix}$$

where $\lambda$ is the switching gain. Considering that the sign function is discontinuous, it will inevitably result in a severe chattering problem. Therefore, for purpose of relieving this situation, the saturation function $\mathrm{sat}(s) = \begin{cases} \lambda & s > k \\ s/k & |s| \le k \\ -\lambda & s < -k \end{cases}$ is commonly employed to replace the sign function. However, this manner will also introduce a relatively large estimation error of the internal back-EMF, although the original chattering is promisingly attenuated.

### B. Phase Detector

It is notable from system (2) that the estimations $\hat{E}_\alpha$ and $\hat{E}_\beta$ inherently contain the rotor position information. Consequently, thus a phase detector (PD) can be utilized to determine the position estimation error, which is depicted as

$$\varepsilon = -\hat{E}_\alpha \cos\hat{\theta}_e - \hat{E}_\beta \sin\hat{\theta}_e = \sqrt{\hat{E}_\alpha^2 + \hat{E}_\beta^2}\sin(e_1) \tag{6}$$

where $e_1 = \theta_e - \hat{\theta}_e$ is defined as the estimation error.

It is obvious from (6) that when $e_1$ gets sufficiently small, the phase displacement can be expressed as

$$e_1 \approx \sin(e_1) = \varepsilon / \sqrt{\hat{E}_\alpha^2 + \hat{E}_\beta^2} \tag{7}$$

With (7) in mind, we can now proceed with the design of the second-stage observer as presented below.

**Remark 3.2:** It is worth noting that this method is specifically designed for PMSM operation in the forward rotation direction. If accurate estimates are required for speed reverse, an alternative approach to consider is the utilization of a dual-phase-locked loop (DPLL), as suggested in reference [12].

### C. Position and Speed Estimation

To proceed, according to the dynamic model (3) and the phase detector (7), the second-stage observer for the position and speed estimations is constructed as the following form:

$$\begin{cases} \dot{\hat{\theta}}_e = \hat{\omega}_e + \iota_1 \lfloor e_1 \rceil^\alpha, \\ \dot{\hat{\omega}}_e = \frac{k_t}{J} i_q^* + \iota_2 \lfloor e_1 \rceil^\beta \end{cases} \tag{8}$$

where $\hat{\theta}_e$ and $\hat{\omega}_e$ are the estimations of $\theta_e$ and $\omega_e$. $\iota_1$, $\iota_2$ are the positive design parameters, $\alpha \in (1/2, 1)$ and $\beta = 2\alpha - 1$.

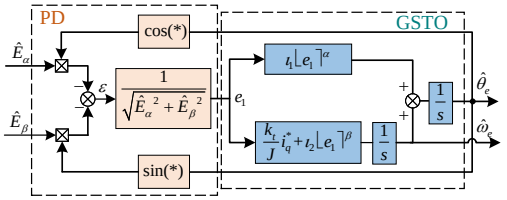


Fig. 2. Structure of position and speed estimation using proposed GSTO.

Fig. 2 shows the block diagram of the second-stage observer.

**Remark 3.3:** The standard approach in conventional SMO is to employ the arctangent function calculation to extract the speed and position, and the specifics can be expressed as

$$\hat{\theta}_e = \arctan\left(-\hat{E}_\alpha/\hat{E}_\beta\right),\ \hat{\omega}_e = \mathrm{LPF}\left(d\hat{\theta}_e/dt, f\right) \tag{9}$$

where $f$ is the cut-off frequency of LPF. Nevertheless, the estimation accuracy highly relies on the waveforms of the back-EMF that may be distorted by inverter nonlinearity, parameter detuning, and measurement noise. The distortion will result in deviation of the phase and frequency. Aiming to cope with this problem, a common manner is to adopt a Q-PLL to track the phase and frequency of the estimated back-EMF, and the expression of the Q-PLL can be described as

$$\begin{cases} \varepsilon = -\hat{E}_\alpha \cos\hat{\theta}_e - \hat{E}_\beta \sin\hat{\theta}_e, \\ \hat{\omega}_e = k_p\varepsilon + k_i \int \varepsilon dt \end{cases} \tag{10}$$

where $k_p$, $k_i$ are the positive gains.

Fig. 3 illustrates the entire architecture of the proposed cascaded GSTO design framework.

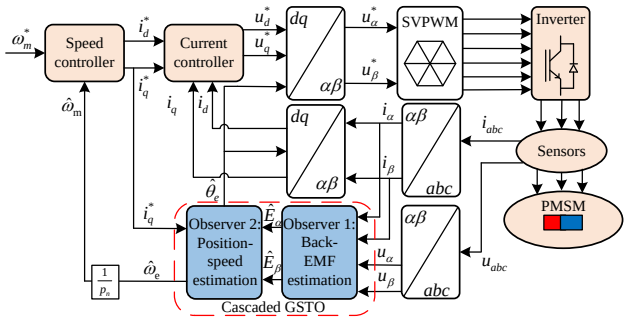


Fig. 3. Diagram of the proposed cascaded GSTO-based sensorless control.

### D. Stability Analysis

A simple theoretical stability analysis is given in this subsection. To begin with, we introduce a key lemma:

**Lemma 1:** [15]: For the following nonlinear system:

$$\begin{cases} \dot{s}_1 = s_2 - \lambda_1 \lfloor s_1 \rceil^{\alpha}, \\ \dot{s}_2 = -\lambda_2 \lfloor s_1 \rceil^{\beta} + d \end{cases} \tag{11}$$

where $\alpha \in (1/2, 1)$, $\beta = 2\alpha - 1$, and $d$ is an unknown and bounded signal. If the positive control gains $\lambda_1$ and $\lambda_2$ are configured properly, the sliding variables $s_1$ and $s_2$ will converge to an arbitrarily small region within a finite time.

A rigorous proof is provided in [15] by utilizing strict Lyapunov stability analysis. Furthermore, the fact can be found in [15] that there exist proper $\lambda_1$ and $\lambda_2$ such that the sliding variables can finite-timely converge to the following region:

$$Q = \left\{ (s_1, s_2) \middle| |s_1| \le \sqrt{2} l_2^{\frac{1}{2-\alpha+\beta}} \left(\frac{l_1 \bar{d}}{\lambda_1(1-\kappa)}\right)^{\frac{1}{\beta}} \left(\frac{1}{\sqrt{\alpha}} + 1\right), \right.$$
$$\left. |s_2| \le \lambda_1 l_2^{\frac{\alpha}{2-\alpha+\beta}} \left(\frac{2}{\alpha}\right)^{\frac{\alpha}{2}} \left(\frac{l_1 \bar{d}}{\lambda_1(1-\kappa)}\right)^{\frac{\alpha}{\beta}} \right\}$$

where $\bar{d}$ is the upper bound of $d$, $l_1$ and $l_2$ are the positive constants that always exist, and $\kappa \in (0, 1)$ is an arbitrarily small constant.

To prove the stability of the proposed two-stage observer, taking $\alpha$-axis as the example, one can derive the error dynamics via (1) and (4) as

$$\begin{cases} \dot{e}_{1\alpha} = e_{2\alpha} - \dfrac{\lambda_1}{L} \lfloor e_{1\alpha} \rceil^{a}, \\ \dot{e}_{2\alpha} = -\dfrac{\lambda_2}{L} \lfloor e_{1\alpha} \rceil^{b} + \dfrac{\dot{E}_\alpha}{L} \end{cases} \tag{12}$$

where $e_{1\alpha} = \hat{i}_\alpha - i_\alpha$ and $e_{2\alpha} = (E_\alpha - \hat{E}_\alpha)/L$.

Simultaneously, define $e_2 = \omega_e - \hat{\omega}_e$. The fact is that when the estimation error gets sufficiently smaller, the dynamic equation of the position estimation error can be derived with the assistance of (3) and (8), which can be depicted as

$$\begin{cases} \dot{e}_1 = e_2 - \iota_1 \lfloor e_1 \rceil^{\alpha}, \\ \dot{e}_2 = -\iota_2 \lfloor e_1 \rceil^{\beta} + d \end{cases} \tag{13}$$

From Lemma 1, it is known that there exist suitable gains of $\lambda_1$, $\lambda_2$ and $\iota_1$, $\iota_2$ such that the estimation errors in (12) and (13) can finite-timely converge to an arbitrarily small region by tuning the gains and fractional power appropriately.

**Remark 3.4:** It is worth pointing out that the cascaded GSTO proposed in this brief is essentially a nonsmooth observer, located between a super-twisting observer and a smooth observer. As the value of $a$ approaches value $1/2$, the behavior of the cascaded GSTO gradually degrades to a cascaded STO. Conversely, as $\alpha$ approaches value 1, the cascaded GSTO could gradually become a cascaded ESO, i.e.,

$$\begin{cases} \dot{e_{1\alpha}} = e_{2\alpha} - \lambda_1 |e_{1\alpha}|^{\frac{1}{2}} \mathrm{sign}(e_{1\alpha}) \\ \dot{e_{2\alpha}} = -\lambda_2 \mathrm{sign}(e_{1\alpha}) \\ \dot{e_1} = e_2 - \iota_1 |e_1|^{\frac{1}{2}} \mathrm{sign}(e_1) \\ \dot{e_2} = -\iota_2 \mathrm{sign}(e_1) \end{cases}, \begin{cases} \dot{e_{1\alpha}} = e_{2\alpha} - \lambda_1 e_{1\alpha} \\ \dot{e_{2\alpha}} = -\lambda_2 e_{1\alpha} \\ \dot{e_1} = e_2 - \iota_1 e_1 \\ \dot{e_2} = -\iota_2 e_1 \end{cases}$$

Furthermore, larger values of $\lambda_1$ and $\iota_1$ imply shorter settling time for the system states and improve dynamic performance, and larger values of $\lambda_2$ and $\iota_2$ indicate better steady-state performance and enhanced anti-disturbance performance.

## IV. Experimental Results

To verify the position estimation performance of the proposed approach, an experimental setup is deployed in the laboratory by utilizing a TMS320F28379D DSP, as depicted in Fig. 4. The control system is configured with a sampling frequency of 16 kHz. It is noteworthy that in this experiment, the motor initially starts with open-loop operation before transitioning to closed-loop control. In this section, a

comparative analysis is implemented by comparing with the SMO-integrated arctan method (SMO+arctan) from (9) and SMO-integrated Q-PLL method (SMO+Q-PLL) from (10). Specifically, we also consider two special cases, i.e., the cascaded ESO and the cascaded STO.

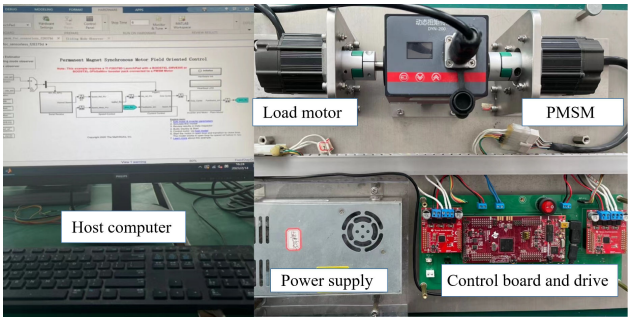


Fig. 4. Experimental setup of the PMSM system.

### A. Parameters Selection

This subsection describes the role of parameters, and to make a fair comparison, for the two traditional methods, trial-and-error solution for the parameters is used to make both methods similar in dynamic and steady-state performance, while for cascaded GSTO, turning $\lambda_1$ and $\iota_1$ up to obtain better dynamic performance of position and speed estimation, turning $\lambda_2$ and $\iota_2$ up to improve the steady-state performance of position and speed estimation, but too much $\lambda_1$ and $\iota_1$ will have an impact on the system stability.

The parameters for these five different estimation strategies are selected as: (1) SMO+arctan: $\lambda = 10$, $f = 65$ Hz; (2) SMO+Q-PLL: $k_p = 1200$, $k_i = 360000$ while $k$ and $\lambda$ are equals to the values in (1); (3) Cascaded ESO: $a = \alpha = b = \beta = 1$, $\lambda_1 = 2$, $\lambda_2 = 20000$, $\iota_1 = 1200$, $\iota_2 = 360000$; (4) Cascaded STO: $a = \alpha = 0.5$, $b = \beta = 0$; (5) Cascaded GSTO: $a = \alpha = 0.75$, $b = \beta = 0.5$, while $\lambda_1$, $\lambda_2$ and $\iota_1$, $\iota_2$ in (4), (5) are equal to the values in (3). The parameters of PMSM to be studied are listed in Table I.

TABLE I
PMSM PARAMETERS

| Parameter | Symbol | Value |
|---|---|---|
| Flux linkage | $\phi_f$ | 0.0064Wb |
| Motor inertia | $J$ | $7.06\times10^{-6}$kg·m$^2$ |
| DC bus voltage | $U_d$ | 24V |
| Rated speed @$U_d$ | $n$ | 4107rpm |
| Maximum speed | $n_{max}$ | 6000rpm |
| Phase resistance | $R$ | 0.36Ω |
| Phase inductance | $L$ | 0.2mH |
| Number of pole pairs | $P_n$ | 4 |
| Rated current | $I$ | 7.1A |

In order to study the performance of the conventional method and the proposed method for the estimation of the back-EMF, a comparison is made between the conventional SMO and the proposed method at different fractional powers. It can be found in Fig. 5 that for the conventional SMO, the estimation of the back-EMF is distorted due to the effect of the discontinuity term, while for proposed method as the $a$ and $\alpha$ get smaller and closer to 0.5, the effect of the discontinuity term becomes larger leading to more noise in the back-EMF, and as the $a$ and $\alpha$ gets larger and closer to 1 the noise in back-EMF becomes smaller. Therefore, the proposed method can effectively reduce the noise in the back-EMF estimation.

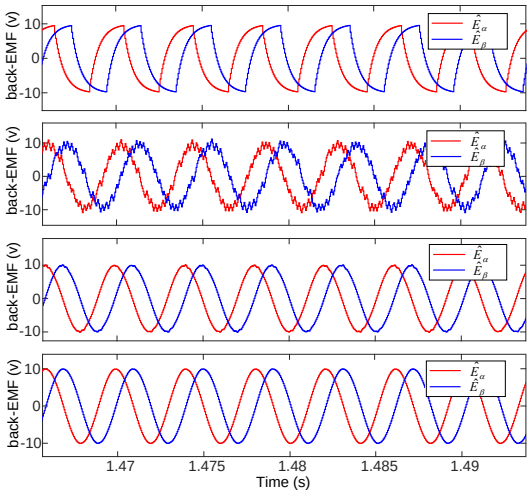


Fig. 5. Back-EMF estimation curves under SMO and three different fractional powers in GSTO: (a) SMO at $\lambda = 10$ (b) $a = 0.6$, $b = 0.2$. (c) $a = 0.75$, $b = 0.5$. (d) $a = 0.9$, $b = 0.8$

### B. Performance Comparisons

In this subsection, the position estimation curves and speed response curves are compared under five methods.

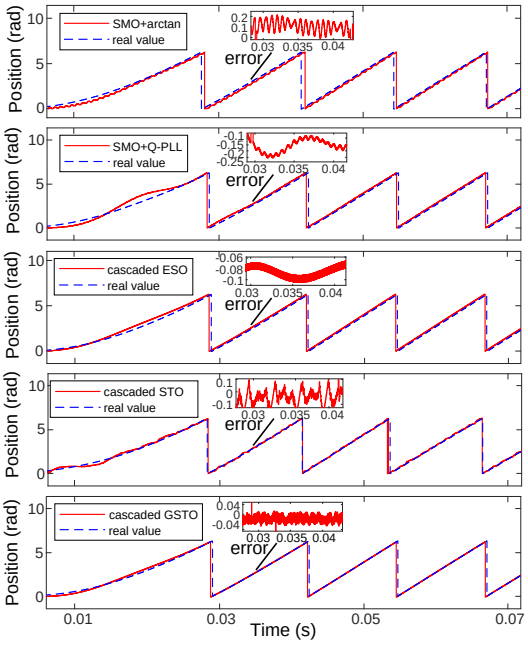


Fig. 6. Position estimation curves under five different strategies.

Fig. 6 depicts the different position estimation results. It can be seen that the two conventional methods, i.e., SMO+arctan and SMO+Q-PLL have relatively estimation error due to its chatting problem, while the cascaded GSTO proposed in this brief has the smallest estimation error. This also means that with the same gain, for different fractional power, the smaller

$a, b$ and $\alpha, \beta$ means that the influence of the discontinuity term is greater and the noise in the back-EMF will have an impact on the position estimation, thus producing a larger estimation error, while larger $a, b$ and $\alpha, \beta$ means that the influence of the discontinuity term is smaller and the estimation error of the position becomes smaller accordingly, but if the fractional power is too large it will cause a static difference in the position estimation.

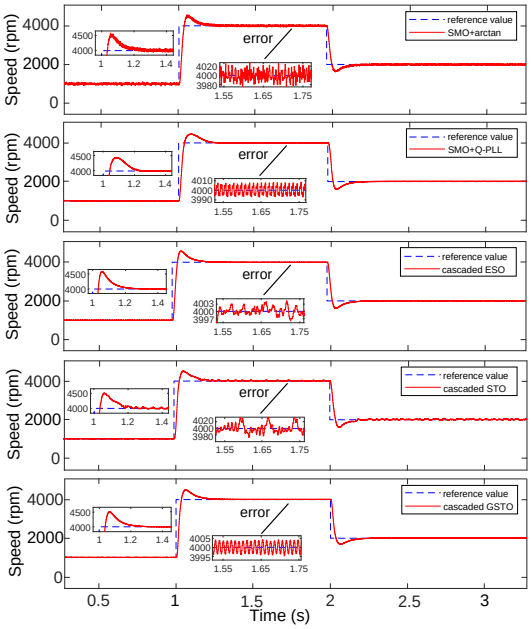


Fig. 7. Speed response curves under five different strategies.

As depicted in Fig. 7, the proposed method exhibits superior dynamic and steady-state performance compared to other approaches. Additionally, the cascaded ESO exhibits the smallest speed fluctuation, at only 6 rpm, but it induces the largest overshoot about the peak of 4580 rpm during the speed transition in 1 second. On the other hand, it is notable that the SMO+arctan method suffers from chattering issues, resulting in a maximum speed fluctuation of 40 rpm after entering the steady state. Furthermore, the cascaded STO method shows the shortest time to reach the steady-state, but it is still affected by the discontinuity term. Consequently, the proposed observation approach needs to balance the trade-off between the overshoot and speed fluctuations by selecting appropriate parameters to achieve better results.

## V. Conclusion

This brief has developed a cascaded GSTO approach aiming to enhance the position estimation performance for sensorless PMSM drives. A two-stage observer was constructed to extract the back-EMF and rebuild the rotor position information respectively. The stability analysis has been studied to ensure the validity of the scheme. Comparative experimental analyses compared with the existing work demonstrate that the proposed method minimizes the high-frequency noise of the back-EMF and provides accurate estimates of rotor position and speed. Future work will focus on extending the proposed method to wide-range speed regulation systems.

## References

[1] D. Xiao, S. Nalakath, S. R. Filho, G. Fang, A. Dong, Y. Sun, J. Wiseman, and A. Emadi, "Universal full-speed sensorless control scheme for interior permanent magnet synchronous motors," *IEEE Transactions on Power Electronics*, vol. 36, no. 4, pp. 4723-4737, 2021.

[2] Z. -X. Fan, S. Li and R. Liu, "ADP-based optimal control for systems with mismatched disturbances: A PMSM Application," *IEEE Transactions on Circuits and Systems II: Express Briefs*, vol. 70, no. 6, pp. 2057-2061, 2023.

[3] S. -K. Kim, Y. Kim and C. K. Ahn, "Energy-shaping speed controller with time-varying damping injection for permanent-magnet synchronous motors," *IEEE Transactions on Circuits and Systems II: Express Briefs*, vol. 68, no. 1, pp. 381-385, 2021.

[4] C. Wang, L. Gou, S. Dong, M. Zhou, and X. You, "Sensorless control of IPMSM based on super-twisting sliding mode observer with CVGI considering flying start," *IEEE Transactions on Transportation Electrification*, vol. 8, no. 2, pp. 2106-2117, 2022.

[5] W. Xu, Y. Jiang, C. Mu, and F. Blaabjerg, "Improved nonlinear flux observer-based second-order SOIFO for PMSM sensorless control," *IEEE Transactions on Power Electronics*, vol. 34, no. 1, pp. 565–579, 2019.

[6] E. Dehghan-Azad, S. Gadoue, D. Atkinson, H. Slater, P. Barrass, and F. Blaabjerg, "Sensorless control of IM based on stator-voltage MRAS for limp-home EV applications," *IEEE Transactions on Power Electronics*, vol. 33, no. 3, pp. 1911-1921, 2018.

[7] S. Ding, K. Mei, and S. Li, "A new second-order sliding mode and its application to nonlinear constrained systems," *IEEE Transactions on Automatic Control*, vol. 64, no. 6, pp. 2545-2552, 2019.

[8] Y. Tan, J. Liu, X. Xie, E. Tian and J. Liu, "Event-triggered sliding-mode control for fuzzy semi-Markovian jump systems with dead zone input and application to circuit systems," *IEEE Transactions on Circuits and Systems II: Express Briefs*, 2023, doi: 10.1109/TCSII.2023.3257088.

[9] C. Sun, S. Wang and H. Yu, "Finite-time sliding mode control based on unknown system dynamics estimator for nonlinear robotic systems," *IEEE Transactions on Circuits and Systems II: Express Briefs*, 2023, doi: 10.1109/TCSII.2023.3243570.

[10] G. Wang, M. Valla, and J. Solsona, "Position sensorless permanent magnet synchronous machine drives—a review," *IEEE Transactions on Industrial Electronics*, vol. 67, no. 7, pp. 5830-5842, 2020.

[11] K. Mei, S. Ding, and W. X. Zheng, "Fuzzy adaptive SOSM based control of a type of nonlinear systems," *IEEE Transactions on Circuits and Systems II: Express Briefs*, vol. 69, no. 3, pp. 1342-1346, 2022.

[12] Z. Chen, A. A. Dawara, X. Zhang, H. Zhang, C. Liu and G. Luo, "Adaptive sliding mode observer-based sensorless control for SPMSM employing a dual-PLL," *IEEE Transactions on Transportation Electrification*, vol. 8, no. 1, pp. 1267-1277, 2022.

[13] Q. Hou and S. Ding, "GPIO based super-twisting sliding mode control for PMSM," *IEEE Transactions on Circuits and Systems II: Express Briefs*, vol. 68, no. 2, pp. 747-751, 2021.

[14] L. Wang, Z. Song, X. Liu, Z. Li, T. Fernando and H. H. C. Iu, "Continuous finite-time integral sliding mode control for attitude stabilization," *IEEE Transactions on Circuits and Systems II: Express Briefs*, vol. 67, no. 10, pp. 2084-2088, 2020.

[15] K. Mei, S. Ding, and X. Yu, "A generalized super-twisting algorithm," *IEEE Transactions on Cybernetics*, 2022, doi: 10.1109/TCYB. 2022. 3188877.

[16] G. Liu, H. Zhang, and X. Song, "Position-estimation deviation-suppression technology of PMSM combining phase self-compensation SMO and feed-forward PLL," *IEEE Journal of Emerging and Selected Topics in Power Electronics*, vol. 9, no. 1, pp. 335-344, 2021.

[17] S. -K. Kim, K. S. Kim, S. Lim, and C. K. Ahn, "Model-free observer for speed and acceleration estimations for speed servo system applications," *IEEE Transactions on Circuits and Systems II: Express Briefs*, vol. 69, no. 12, pp. 4944-4948, 2022.

[18] Z. Xu, T. Zhang, Y. Bao, H. Zhang, and C. Gerada, "A nonlinear extended state observer for rotor position and speed estimation for sensorless IPMSM drives," *IEEE Transactions on Power Electronics*, vol. 35, no. 1, pp. 733-743, 2020.

[19] C. Zhang, J. Yang, Y. Yan, L. Fridman, and S. Li, "Semiglobal finite-time trajectory tracking realization for disturbed nonlinear systems via higher-order sliding modes," *IEEE Transactions on Automatic Control*, vol. 65, no. 5, pp. 2185-2191, 2019.

[20] J. Mao, S. Li, Q. Li, and J. Yang, "Design and implementation of continuous finite-time sliding mode control for 2-DOF inertially stabilized platform subject to multiple disturbances," *ISA Transactions*, vol. 84, pp. 214-224, 2019.